ELSEVIER

International Journal of Mass Spectrometry 192 (1999) 49–63

International Journal of Mass Spectrometry

Multiple *K*- and *L*-shell ionizations of target atoms by collisions with high-energy heavy ions

Y. Awaya*[,1], T. Kambara, Y. Kanai

The Institute of Physical and Chemical Research (RIKEN), Wako, Saitama 351-0198, Japan

Received 9 December 1998; accepted 19 April 1999

Abstract

The inner-shell ionization processes of atoms by bombardment of fast heavy ions are studied systematically through high-resolution measurements of *K* x rays. The K_α satellite and K_α hypersatellite x rays from target *K*-shell ionization were measured for He, C, N, O, and Ar-ion impact at energies between 0.56 and 92 MeV/u for satellite x rays and between 4.7 and 92 MeV/u for hypersatellite x rays. From the intensity distribution of the K_α satellite x rays with a different number of *L*-shell vacancies, the *L*-shell ionization probability at small impact parameters (close collisions) have been obtained and the results are discussed in the framework of simple first-order theories like binary-encounter approximation (BEA), and semiclassical approximation (SCA). The results qualitatively agree with the BEA and SCA scalings at higher collision velocities than the orbital velocity of the *L* electrons. The intensity ratio between K_α hypersatellite x rays and K_α satellite x rays has been compared with results calculated by BEA and SCA. (Int J Mass Spectrom 192 (1999) 49–63) © 1999 Elsevier Science B.V.

Keywords: *K*-shell ionization; Double *K*-shell ionization; Inner-shell ionization; Multiple ionization; Heavy ion-atom collision; *K* satellite x-rays; *K* hypersatellite x-rays; Binary encounter approximation; Semiclassical approximation

1. Introduction

In fast ion–atom collisions, the production of a *K* vacancy in the projectile or target atom can be accompanied by the production of another *K* vacancy or one or more *L* vacancies in the same atom. The *K* x rays from decays of excited states with such multiple innershell vacancies have higher energies than that from a single *K*-vacancy state. Therefore, x-ray spectra from the collisions have satellite and hypersatellite structures that can be observed in high-resolution x-ray measurements. Hereafter we denote an atomic state with *m K* vacancy and *n L* vacancies as a K^mL^n state ($m \leq 2$, $n \leq 7$) and *K* x rays from this state as KL^n x rays for $m = 1$ (satellites) and a K^2L^n x rays for $m = 2$ (hypersatellites). The multiple inner-shell ionization of a target atom is largely enhanced by heavy-ion impact. Such enhancement was observed as a energy shift of the *K* x rays in low-resolution measurements [1], and then in KL^n x-ray intensity distribution in high-resolution measurements [2,3]. Since such enhancement was first observed, many studies have been made on this subject [4–7]; the dependence of the structure of the KL^n x-ray spectra on the energy, atomic number and charge state of the projectile ions, the atomic number

* Corresponding author.

[1] Present address: Musashino Art University, Ogawa, Kodaira, Tokyo 187-8505 Japan. E-mail: awaya@musabi.ac.jp

PII S1387-3806(99)00097-4

of the target atom, and physical or chemical conditions of the target.

Olsen and Moore [8] measured K^2L^n x-ray spectra by using high resolution spectrometer and compared the intensity distributions of the K^2L^n x rays with the KL^n x rays.

If multiple ionization is treated as simultaneous independent single ionization of the orbital electrons and the electron correlation effects are neglected, the multiple-ionization probability can be expressed by the single-electron ionization probabilities. If all the L electrons have the same ionization probability, the cross section of simultaneous single K and n-fold L ionization is expressed as

$$\sigma_{K,nL} = \int_0^\infty 2\pi b 2P_K(b)\binom{8}{n}P_L(b)^n \times [1 - P_L(b)]^{8-n}\, db \quad (1)$$

where $P_K(b)$ and $P_L(b)$ are the single K and L ionization probabilities as functions of the impact parameter b. Since $P_K(b)$ has nonzero values only at small impact parameters where the b dependence of $P_L(b)$ is not significant, $P_L(b)$ in the above equation can be replaced by a constant $P_L = P_L(0)$. Then the multiple L-ionization cross section has a binomial distribution:

$$\sigma_{K,nL} = \sigma_K\binom{8}{n}P_L^n(1 - P_L)^{8-n} \quad (2)$$

where σ_K is the K-ionization cross section. The value of P_L is obtained from relative cross sections to produce different numbers of L vacancies simultaneously with a K-vacancy production, which can be deduced from the intensity distributions of the KL^n x rays.

The impact parameter dependence of inner-shell ionization probabilities are often studied through coincidence measurements between characteristic x rays or Auger electrons and the deflection of the projectiles by nuclear coulomb scattering. These kind of measurements usually offer more detailed information on the inner-shell ionization probabilities than the high resolution measurements of x rays with a crystal spectrometer. But at the coincidental measurements we have to prepare a very finely collimated beam so as to determine a very small scattering angle, especially at high projectile energy. This makes it difficult to make systematic studies of impact parameter dependence of inner-shell ionization. On the other hand, for the measurement of KL^n x-ray distribution, we can use a same x-ray crystal spectrometer for different collision systems and velocities, where the coincidence measurements are difficult because of small scattering angle. We have investigated many collision systems and a wide range of collision velocities systematically by using this equipment to test the validity of theories and general scaling laws as functions of the parameters describing the collision system; the atomic number of the projectile (Z_1), the target (Z_2), and the collision velocity (v_i).

Several experimental studies have been reported on systematics of L- and M-shell ionization probabilities through measurements of KL^n x-ray intensity distribution. The results have been compared with first-order direct coulomb ionization models, like the plane-wave Born approximation (PWBA), semiclassical approximation (SCA), or binary encounter approximation (BEA).

Kauffman et al. [4] studied projectile and target dependences with 0.8 MeV H, 3.2 MeV He, and 30 MeV O ions on targets of Ca, Sc, Ti, V, Cr, and Mn. They found that the relative cross sections of the multiple L-vacancy production followed a binomial distribution, and BEA calculations qualitatively reproduced the experimental P_L values for proton and He projectiles, whereas crude SCA calculations overestimated them. They also found that the BEA calculations significantly overestimate the P_L values for the O-ion projectile.

Richard et al. [5] studied collision energy dependence of ionization cross sections for the KL^n states with 0.4–3.0 MeV He ions on an Al target. A BEA calculation reproduces the gross feature of their experimental results, but some discrepancies were found between them, especially in the position of the extrema of the cross sections.

Schmiedekamp et al. [6] studied projectile dependences of KL^n x-ray intensities of Ar gas target

excited by 1–5 MeV/u H, C, N, O, F, Si, and Cl ions on Ar. They compared the results of the P_L to BEA and PWBA universal functions and found agreements when velocity-dependent binding corrections were introduced. They also evaluated the influence of the rearrangements of the vacancies by *LMM* Auger transitions prior to the x-ray emission on the P_L.

Awaya et al. [11] reported the first systematic experimental study of the *L*- and *M*-shell ionization probabilities P_L and P_M as functions of all the parameters Z_1, Z_2 and v_i with projectiles of He, C, N, and O at energies between $4.7 \leq E \leq 8.2$ MeV/u. The targets used for the P_L measurements were Al, Ar, Ti, Cr, Fe, Ni, Kr, and Y, and those for the P_M measurements were Y, Mo, Ag, and Sn. The results agreed well with a BEA scaling.

Systematic studies on the double *K*-ionization process are only a few. Olsen and Moore [8] measured Ca hypersatellite x-ray spectra induced by O ions of energy from 24 to 48 MeV, as well as the satellite x rays. They studied the P_L for both the satellite and hypersatellite lines.

Fujimoto et al. [9] studied the Be x-ray spectra induced by proton and He projectiles with energies from 0.5 to 2.0 MeV by using a crystal spectrometer. They observed the hypersatellite lines for He impact and studied the incident energy dependence of hypersatellite x-ray production cross section. Kawatsura et al. [10] studied projectile atomic number dependences of double ionization in Be, B, and O atoms by protons, H_2^+, and He^+ ions whose energies ranged from 0.25 to 2.0 MeV. They found that the double *K* ionization cross section depends upon Z_1^4.

Awaya et al. studied the intensity ratio of hypersatellite X-rays to satellite x rays, $I = \Sigma X(K^2L^n)/\Sigma X(KL^n)$, where $X(K^2L^n)$ and $X(KL^n)$ are the yield of K^2L^n and KL^n x rays, respectively, for the projectiles whose incident energy ranged from 4.7 to 7.7 MeV/u [13]. They reported *I* is well proportional to Z_1^2, for the collision system of 6 MeV/u projectiles of $Z_1 = 2$, 6, 7, and 8 on a Ti target.

Here we present systematic investigation of the *L*-shell ionization probability P_L of the target atoms and systematics of intensity ratio between hypersatellite and satellite x rays by close collisions with heavy ions as an extension of the previous works at RIKEN. The study includes the dependences of P_L on the Z_1, Z_2, and v_i, in a wider range of Z_1 and v_i, measured in the same experimental setup as before, then we have been able to get systematic data for a very wide range of projectile energy for the first time. We compare the results of single *K* and *n L* ionization with simple scaling laws predicted by theoretical models of direct coulomb ionization, and study the applicability and limitation of them to various collision systems according to the collision velocity. The theoretical models applied here are BEA and SCA in which impact parameter dependent formulation are available.

We had a special interest in asymmetric collisions at velocities lower than the target *L*-electron velocity v_L and near-symmetric collisions at velocities much higher than v_L.

When the nucleus of the projectile approaches the target nucleus during the collision, the time-dependent coulomb force by the projectile distorts the wave function of the target electron and thus changes the ionization probabilities. These effects are called binding and polarization effects: The binding effect is more important at small impact parameters whereas the polarization is important at large impact parameters. These effects influence the ionization probability significantly at velocities lower than the orbital electron velocity and for higher Z_1 to deviate them from the first-order theories. We have made measurements with slow ($4.8 \leq v_i \leq 9.8$) N ions and studied the binding effect in a SCA.

These first-order theories are usually not applied for nearly symmetric collisions ($Z_1 \sim Z_2$) where the electron orbits of the collision partners are strongly deformed during close collisions. However, it is expected that at high collision velocities the ionization process in nearly symmetric collisions can be described by the same first-order theories as the asymmetric case. We have made measurements with fast (56.8 a.u.) Ar ions on Ti, V, Fe, Ni, and Cu targets and compared the results with those of lower-velocity light-ion collisions.

On the double *K* ionization, we measured the *I* values for the 26 MeV/u N ions and 92 MeV/u Ar ions. Together with the previous data [13], we will

Table 1
Projectile–target combinations and collision energies that were studied

Projectile	Target	Energy (MeV/u)
N	Cr	0.56, 0.82, 1.1, 1.5, 2.1, 2.4
N	Ti	0.81, 0.84, 1.09, 1.3, 1.5
He, O	Ti	6.0
C	Ti	5.1, 6.0, 6.8, 4.7, 4.9
N	Ti	4.7, 5.1, 6.0, 6.8, 7.7
N	Cr, Fe, Ni, Y	6.0
N	Ar	5.0, 5.3, 5.6, 5.8, 6.0, 6.2, 7.6, 7.8
N	Ti, Fe, Ni, Cu	26
Ar	Ti, V, Fe, Ni, Cu	92

discuss the projectile energy dependence of the I values, which is roughly approximated to the ratio of the double to the single K ionization cross section.

Atomic units are used in the following sections unless otherwise specified.

2. Experiments

Heavy-ion beams were produced by three accelerators of RIKEN: 4.7–8.2 MeV/u He, C, N, and O ions were produced by an ordinary 160 cm cyclotron, 0.56–2.4 MeV/u N ions by a heavy-ion linear accelerator (RILAC), and 26 MeV/u N ions and 92 MeV/u Ar ions by a ring cyclotron (RRC). The collision velocity ranges from 3.5% to 41% of the speed of light, c, or from 4.8 to 56.8 a.u. Table 1 summarizes the collision systems which we have investigated. Part of the works at the 160 cm cyclotron and a part of preliminary results at the RILAC and the RRC have been reported elsewhere [7,11–14].

Most of the solid targets were self-supported metallic foils with a thickness of a few micrometers. The energy loss of the ions in the targets are less than 6% of the incident energy $E \geq 4.7$ MeV/u. At lower energies, $E \leq 2.4$ MeV/u, the energy loss is large for thick targets. Actually at projectile energies of 0.8–1.5 MeV/u in the 2 μm thick Ti target, the spread is estimated to be 4–5 MeV which is about 20%–50% of the incident energy. To avoid this problem, we used targets of Cr with thicknesses of about 60 μg/cm^2 evaporated on a mylar foil and about 20 μg/cm^2 on a C foil, impinged by a N-ion beam at 0.56–2.4 MeV/u. The largest energy spread due to the energy loss was about 4% of the incident energy. The Ar target was contained in a gas cell with windows for the entrance and exit of the ion beam [7]. The energy of the ions at the position of x-ray measurement in the gas cell was estimated from the incident energy, the energy loss by the entrance window and that by the gas before the position for each run.

The K x rays from the target elements were measured with a broad range crystal spectrometer [15] placed at 90° to the beam to resolve the K_α x rays to the KL^n and K^2L^n components. The crystal spectrometer consists of a gas-flow position sensitive proportional counter (PSPC) and a flat crystal. A crystal of Ge(111) was used for Ti x rays and that of LiF(200) or LiF(220) for Cr, Fe, Ni, and Cu x rays. In addition to this spectrometer, a step-scanning crystal spectrometer was used in experiments at the 160 cm cyclotron.

Some examples of the Ti x-ray spectra are shown in Fig. 1. Peaks are labeled according to the vacancy configuration of the states before the emission of x rays. Peaks around 4.5 keV are the KL^n_α x rays, and those around 4.9–5.0 keV are the KL^n_β x rays. Small peaks around 4.7 keV are hypersatellites ($K^2L^n_\alpha$ x rays).

3. Single K-shell ionization

We have analyzed all the K x-ray spectra data from the experiments in a same procedure for a consistency. The old data have been re-analyzed.

3.1. Experimental results

3.1.1. Corrections for fluorescence yields

We have fitted the KL^n_α x-ray spectra with a sum of Gaussian functions on a smooth background by using least-squares method to obtain the intensity distributions among the components, and corrected each of the KL^n x-ray intensities for its fluorescence yield to get the relative cross sections of the single K and multiple L ionization. For the correction, we needed

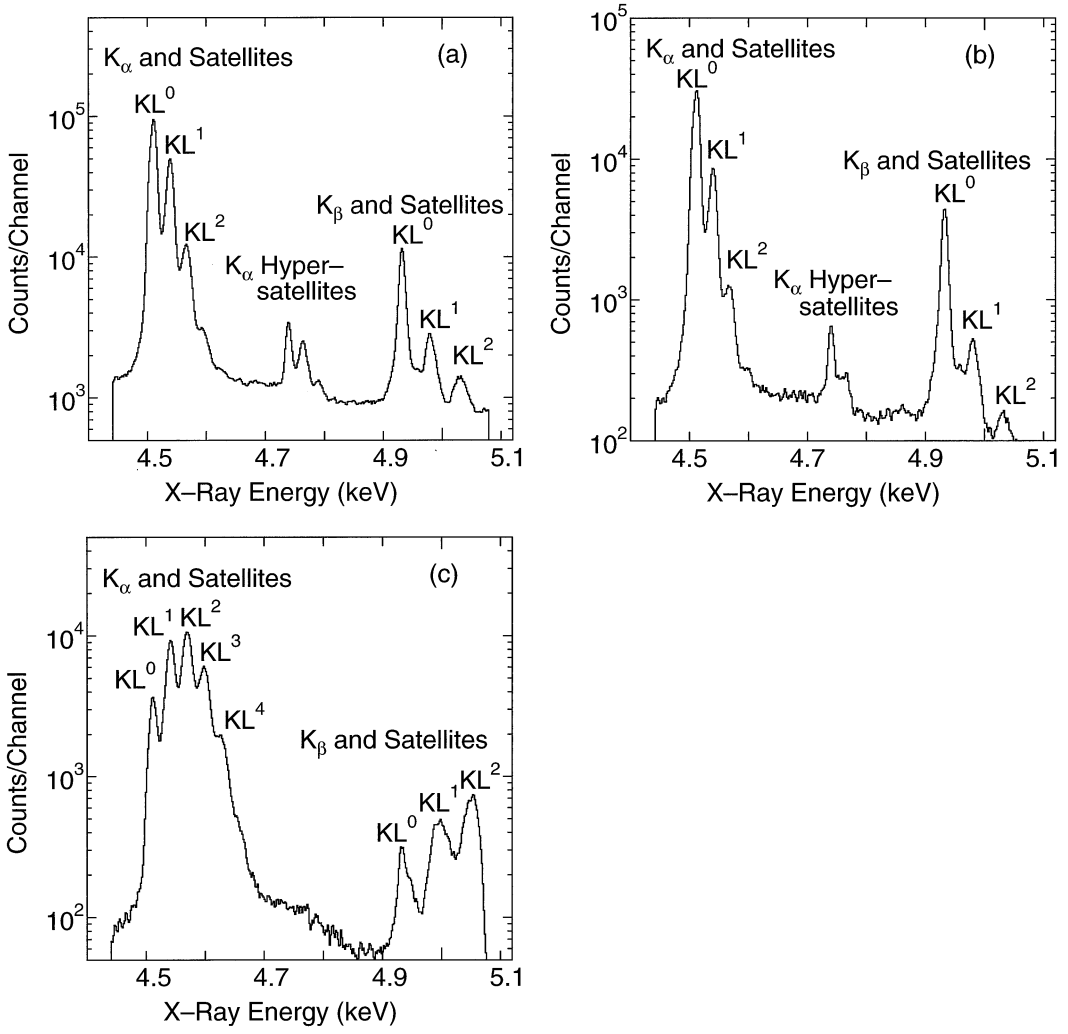

Fig. 1. Spectra of K x rays from a Ti target excited by (a) Ar ions at 92 MeV/u and N ions at (b) 26 MeV/u and (c) 1.3 MeV/u.

values of fluorescence yield for states with a K vacancy and different numbers of L vacancies of different elements. Although there are plenty of experimental and theoretical fluorescence yields for neutral atoms, and detailed calculations for several ions with inner-shell vacancies, they are not enough for our purpose, since the fluorescence yield depends on the electronic configuration of the L shell and the atomic number. We have adopted a scaling technique given by Larkins [16], with values of radiative transition rate by Scofield [17] and those of Auger rate by Chen et al. [18]. The corrections for the fluorescence yield changes the value of P_L within 10% in the case of the Ti target.

In the present case, we are interested in the relative cross sections of the KL^n states, therefore the relative values of the fluorescence yield among these states are more important than their absolute values. We have compared the fluorescence yields of Ar from the scaling technique mentioned above with that from detailed calculation by Bhalla [19] for each L vacancy configuration. Although the absolute values of the fluorescence yield for KL^n ($n \leq 4$) states differ by about 3%–5%, the ratio of that for KL^n satellite to the

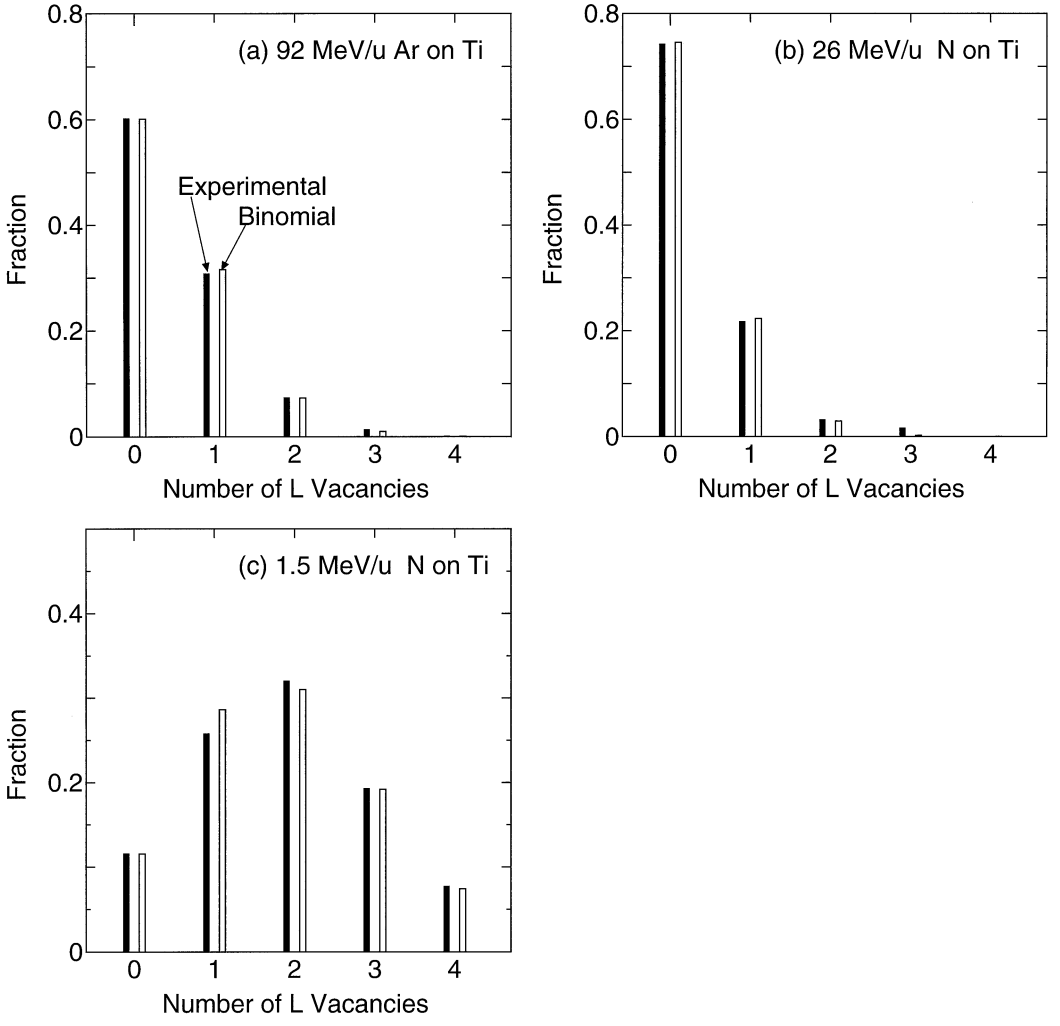

Fig. 2. Distribution of KL_{α}^{n} x-ray intensities of a Ti target excited by (a) Ar ions at 92 MeV/u and N ions at (b) 26 MeV/u, and at (c) 1.5 MeV/u. Solid bars show the experimental data and white bars, the best-fit values to a binomial distribution.

KL^0 transition is smaller than 3%, and the effect of this difference on the results of the P_L value is about 1%.

Schmiedekamp et al. [6] discussed the effect of electron rearrangement due to the *LMM* Auger effects after the ionization and before the *K* x-ray emission by model calculations and concluded that the change of P_L is within $\pm 10\%$ if the *M*-shell vacancy production probability is not very small. We have made no corrections for the rearrangement effects on the present data.

3.1.2. KL^n intensity distribution

Fig. 2 shows the distribution of the KL^n x-ray intensities, corrected for the fluorescence yield, for Ti $K\alpha$ x rays excited by N ions with different energies.

The intensity distributions among different *n* are fitted to binomial distributions given by Eq. (2) to find the optimum values of P_L. The binomial distributions with the best-fit values of P_L are also shown in Fig. 2. The binomial distribution can reproduce the experimental results in wide range of projectiles, targets, and collision velocities. It supports the idea that the

Table 2
Average ionization probability P_L and the intensity ratio I between hypersatellite and satellite x rays obtained from the measurements for each combination of projectile, target, collision velocity, and energy in the laboratory system; the collision velocity is shown in atomic units

Projectile	Target	Energy (MeV/u)	v_i(au)	P_L	I
He	Ti	6.00	15.5	0.0086	
C	Ti	5.08	14.3	0.113	0.019
		6.00	15.5	0.102	0.021
		6.75	16.4	0.0894	0.022
N	Ar	4.71	13.7	0.173	
		4.86	13.9	0.166	
		5.00	14.1	0.168	
		5.29	14.5	0.164	
		5.52	14.9	0.155	
		5.86	15.3	0.150	
		5.96	15.4	0.149	
		6.14	15.7	0.152	
		7.64	17.4	0.125	
		7.86	17.7	0.121	
	Ti	0.807	5.70	0.196	
		0.836	5.80	0.199	
		1.093	6.63	0.227	
		1.30	7.23	0.237	
		1.50	7.77	0.237	
		4.71	13.7	0.153	0.023
		5.07	14.2	0.146	0.026
		6.0	15.5	0.129	0.027
		6.79	16.5	0.118	0.029
		7.71	17.5	0.102	0.032
		26	31.7	0.0353	0.014
	Cr	0.561	4.75	0.1300	
		0.821	5.75	0.167	
		1.10	6.65	0.199	
		1.50	7.77	0.213	
		2.10	9.19	0.203	
		2.40	9.82	0.196	
		6.0	15.5	0.116	0.023
	Fe	6.0	15.5	0.0940	0.017
		26	31.7	0.0262	0.013
	Ni	6.0	15.5	0.0870	0.012
		26	31.7	0.0289	0.015
	Cu	26	31.7	0.0248	0.015
	Y	6.0	15.5	0.082	
O	Ti	6.0	15.5	0.157	
Ar	Ti	1.27	7.15	0.373	
		92	56.8	0.0635	0.024
	V	92	56.8	0.0623	0.020
	Fe	92	56.8	0.0463	0.029
	Ni	92	56.8	0.0498	0.024
	Cu	92	56.8	0.0429	0.025

multiple ionization of the L-shell electrons proceeds independently of each other, without large effects of electron correlation. Table 2 lists the best-fit value of P_L for each combination of the projectile, target, and the collision energy which we have investigated. For the targets with $Z_2 \leq 24$, the overall error of the P_L is within 5%. For heavier targets, the energy difference between the $K_{\alpha 1}$ and $K_{\alpha 2}$ x rays approaches the

width of the lines. Therefore the structure of the x-ray spectra becomes more complicated. For these targets the error of the P_L is nearly 20%.

3.2. Binary encounter approximation

The BEA is an impulse approximation where an ionization is treated as a classical binary coulomb scattering between the projectile and a quasi free target electron.

In 1965, Gryziński [20,21,22] presented a basic formulation of BEA; a classical treatment of binary collisions, its application to coulomb scattering and formula of ionization cross sections by charged particles. He also gave a simple scaling law to express the ionization cross section σ of an electron in a shell with a principal quantum number n:

$$\sigma = (N\pi Z_1^2/u_n^2)G(V) \tag{3}$$

where N is the number of the electrons in the shell, u_n is the binding energy of the target electron, and $G(V)$ is a universal function of a scaled collision velocity $V = v_i/v_n$ where $v_n = \sqrt{2u_n}$. McGuire and Richard [23] applied the BEA with a universal function of Gerjuoy-Vriens-Garcia [24] (GVG) to calculate the ionization probabilities at small impact parameters. They assumed that the impact parameter dependence of the ionization probability $P_n(b)$ was a step function of b:

$$P_n(b) = \begin{cases} \sigma/(N\pi R_c^2) & \text{if } b < R_c \\ 0 \quad \text{otherwise} \end{cases} \tag{4}$$

with a cutoff radius R_c independent of the collision velocity:

$$R_c = \sqrt{2}n^2/Z_{\text{eff}} \tag{5}$$

where $Z_{\text{eff}} = n\sqrt{2u_n}$ is an effective target nuclear charge. The scaling for the ionization probability P_n of one electron is then given as

$$n^2 u_n P_n/Z_1^2 = G(V). \tag{6}$$

The L-shell ionization P_L is thus scaled as $4u_L P_L/Z_1^2$.

In Fig. 3, the scaled P_L values from all of our measurements are compared with the GVG universal curve as well as a Thomson curve which will be described later. The scaled velocity V ranges between 0.7 and 9.5 relative to the target L-shell electrons.

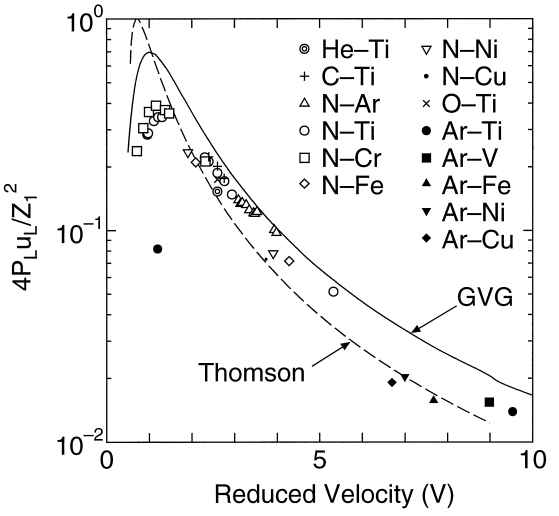

Fig. 3. Scaled L-shell ionization probabilities of target atoms by heavy-ion projectiles are plotted against the scaled velocity $V = v_i/\sqrt{2u_n}$. Closed marks show the experimental data with Ar projectile. The solid line shows the universal GVG curve and the dashed line shows the Thomson curve.

The overall behavior of the scaled experimental P_L values for different collision systems agree the GVG curve for $2 < V < 6$, although the GVG curve is higher, by about 20%, than the experimental values. At the lower and higher velocities, the experimental P_L is apparently lower than the GVG curve.

The experimental P_L values for the Ar gas target come into line with those of the other solid targets like Ti and Fe, therefore we found no indication of solid–gas effects in the present conditions. This is consistent with an investigation by Schmiedekamp et al. [6] who reported that the solid–gas difference in the KL^n distribution is evident for targets with $Z_2 \leq 16$ but small for Ar and heavier targets.

At low velocities, $V < 1.6$, behavior of the experimental data is not much different from the GVG prediction: The experimental data have a maximum at about $V = 1.15$ whereas the BEA prediction has a maximum at $V = 1$. However, the scaled P_L from the BEA predictions are larger than the experimental data

by a factor of about 2, as shown in Fig. 3. The ratio is larger at small collision velocities.

Since we observe collisions at impact parameters smaller than the L-shell radius, the L electrons feel the projectile nuclear charge in addition to the target nuclear charge during the collision and are bound more tightly. This binding effect as well as the effect of deflection of projectile ions by Coulomb scattering strongly influence the ionization cross section when the collision velocity is smaller than the orbital electron velocity. Corrections for these effects are discussed on the basis of Born approximation [25,26]. However, it is not appropriate in view of consistency to incorporate these corrections to the classical BEA model. The binding effect is further discussed in Sec. 3.3 with SCA.

We have made measurements at a high velocity with a 92 MeV/u Ar beam on targets of Ti, V, Fe, Ni, and Cu. The corresponding scaled velocities V are higher than 6.

As this projectile velocity is comparable to the speed of light, (about $0.41c$), we consider here the relativistic effects in a BEA model, from both the kinematics of binary collision and the coulomb scattering cross sections. Since $v_i \gg v_n$, we adopt a simplified model where the initial target electron is at rest and the electrons with a higher recoil energy than the binding energy are ionized by the collision. In the nonrelativistic case, this results in a total cross section formula, given by Thomson:

$$\sigma = \frac{N\pi Z_1^2}{u_n^2 V^2}\left(1 - \frac{1}{4V^2}\right) \tag{7}$$

This corresponds to a universal curve

$$G(V) = \frac{1}{V^2}\left(1 - \frac{1}{4V^2}\right) \tag{8}$$

in Eq. (3) and is shown in Fig. 3 by a dashed curve.

When the energy transfer to the electron is evaluated from a relativistic kinematics and a relativistic Rutherford cross section is adopted, the total ionization cross section is almost same as the nonrelativistic one:

$$\sigma = \frac{N\pi Z_1^2}{u_n^2 V^2}\left[1 - \frac{1-\beta^2}{4V^2}\right] \tag{9}$$

with $\beta = v_i/c$. Although a quantum mechanical Mott cross section is preferable to the classical Rutherford cross section in this case, the difference between these cross sections is within 10% at most of the scattering angle for our cases [27]. Thus the scaling Eq. (3) approximately holds in the present case if the velocity is scaled by $V = v_i/\sqrt{2u_n}$.

As shown in Fig. 3, the experimental results of P_L in this velocity range are lower than the GVG universal curve by about 20%–50%, and tend to agree better with the Thomson curve. We cannot determine whether this behavior is caused by the deviation of the L-shell ionization cross section from the GVG to meet the Thomson curve at these high velocities, or by the slow dependence of the cutoff radius R_c in Eq. (4).

3.3. Semiclassical approximation

The SCA is a perturbation theory with a classical projectile trajectory [28]. We adopted two SCA calculations and compared the results with experimental data for the Ti target: (1) Hansteen et al. [29] proposed a table of impact parameter dependent probabilities of ionization for proton impact. The calculation includes a straight-line trajectory approximation. We have calculated the total L-shell ionization probability from the probabilities for $L1$, $L2$, and $L3$ subshells at the smallest impact parameter on the table. Hereafter this calculation is referred as SCAH. (2) Trautmann and Rösel [30] presented a computer code for full numerical calculation which includes a Coulomb trajectory. We calculated the ionization probabilities for the $L1$, $L2$, and $L3$ subshells for a N–Ti collision system at a impact parameter of 200 fm. In the calculations, we assumed relativistic hydrogenlike wavefunctions for the target electrons, took a recoil effect into account, and included multipoles up to $l = 3$. Since in the calculation the target L-electron wave function is given by the screened nuclear charge of the target atom Z_{2L}, we study the binding effect by comparing the following two cases; $Z_{2L} = Z_2 - 4.15$ where binding effect is not con-

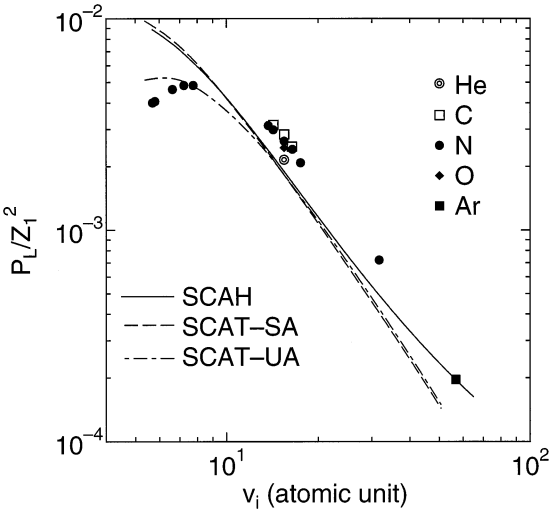

Fig. 4. L-ionization probabilities for one electron P_L of a Ti target bombarded by He, C, N, O, and Ar ions, divided by square of projectile atomic number (Z_1^2). The solid line shows SCA calculation results with a straight-line trajectory for proton impact (SCAH) [29]. The dashed line shows a full SCA calculation for nitrogen impact [30] with separated-atom target wave function (SCAT-SA) and the dot-dashed line shows that with a united-atom wave function (SCAT-UA).

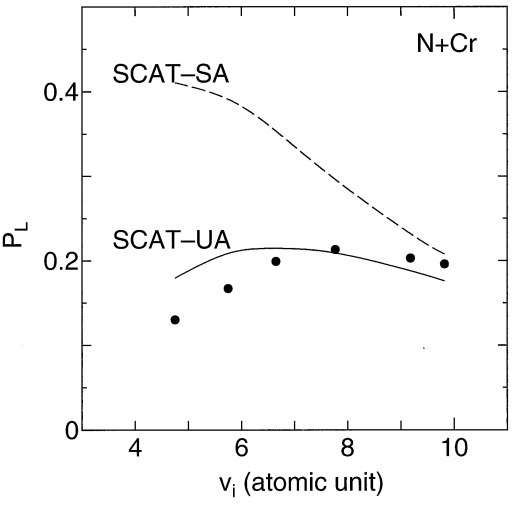

Fig. 5. P_L of a thin Cr target bombarded by N ions. The lines show full SCA calculation for nitrogen impact [30]; solid line for the united-atom calculation (SCAT-UA) and dashed line for the separated-atom calculation (SCAT-SA).

sidered (separated atom; SA) and $Z_{2L} = Z_1 + Z_2 - 4.15$ where binding effect is considered (united atom; UA). The former is hereafter referred as SCAT-SA and the latter as SCAT-UA.

To compare the ionization probabilities by different projectiles, we normalized them to that of one L electron by proton impact with the same velocity: The experimental P_L values are divided by Z_1^2.

Fig. 4 shows the experimental and calculated L-ionization probabilities against the collision velocity v_i in atomic units. The L-electron orbital velocity $v_L = (Z_2 - 4.15)/2$ is about 8.9.

At $v_i > v_L$, these SCA predictions show similar behavior, although the SCAH is higher than SCAT-SA and SCAT-UA at $v_i > 30$. These SCA results are lower than the experimental data by about 20%–30%, but reproduces well the general behavior of the data for different projectiles from He to Ar. It is notable since the experimental results were normalized by a factor Z_1^{-2} which ranges between 1/4 for He and 1/324 for the Ar impact. Similar results have been reported by Rymuza et al. [31] where the projectile K-shell ionization cross sections measured for 80–200 MeV/u Bi ions on C, Al, and Ni targets are higher than the SCA predictions by about 50%.

At $v_i < v_L$, the experimental results are significantly lower than the SCAT-SA and SCAH, and tend to follow the SCAT-UA. This implies the importance of the binding effect at these velocities. However, with a few micrometers thick Ti target, the observed P_L is averaged over the projectile energy spread due to the energy loss in the target. To minimize effect of the energy spread, we made measurements with the thin Cr targets evaporated on C and mylar foils as was described in Sec. 2. Fig. 5 shows the results of P_L for the Cr targets compared with the SCAT-SA and SCAT-UA calculations. The experimental results well follow the SCAT-UA prediction at $v_i < v_L = 10$. It shows that the influence of the binding effect is well reproduced by the SCAT-UA calculation.

As is shown in Fig. 4, the SCAT-UA merges the SCAT-SA prediction above $v_i = 10$ and the P_L/Z_1^2 have almost same values for four different projectiles (He, C, N, and O) with the same velocity $v_i = 15.5$ (about 6 MeV/u). The binding effect seems to vanish at higher collision velocities.

The binding effect has been studied by some

authors with measurements of impact parameter dependence of ionization probabilities. Schuch et al. [32] measured the *K*-ionization probability in 1 MeV/u He on Ca collisions and found that the experimental probabilities at impact parameters smaller than the *K*-shell radius can be reproduced by SCA calculations if the UA is used to calculate the target *K*-shell wave function. Same calculation with SA reproduces the experimental probability at larger impact parameters. Similar effect was observed for *L*-shell ionization of Au by 1 MeV/u Ar ions [33]. However, the effect has been investigated at a given collision system at one projectile velocity. This is the first systematic observation of the binding effect as a function of the collision velocity.

In the BEA described previously, the ionization probability P_L is related to the total cross section in Eq. (3) with an assumption of step function [Eq. (4)] where the cutoff radius is independent of the collision velocity [Eq. (5)].

To check the validity of the assumption, we compared the cutoff radius R_c in Eq. (5) with an average radius $R_{\mathrm{SCA}} = \sqrt{\sigma_{\mathrm{SCA}}/\pi P_{\mathrm{LSCA}}}$, which is deduced from the total *L*-shell ionization cross section σ_{SCA} and the P_L at small impact parameters with the SCA program [30] for N–Ti and N–Cu systems at collision energies between 10 and 1000 MeV. The ratio R_{SCA}/R_c, as seen in Fig. 6, slowly increases with the collision velocity, and is almost same for the two targets. Although the absolute value of the cross section σ is different by a factor of 36 between 10 and 1000 MeV for the N–Ti system, the increase of the ratio R_{SCA}/R_c is 38%. This supports the simplification used in the BEA approximation.

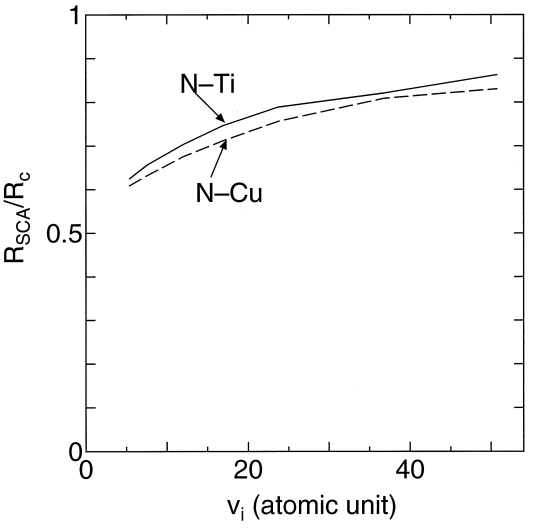

Fig. 6. The ratio between average radius $R_{\mathrm{SCA}} = \sqrt{\sigma_{\mathrm{SCA}}/\pi P_{\mathrm{LSCA}}}$ calculated with a SCA program by Trautmann and Rösel [30] and the cutoff radius R_c in Eq. (5) for collision systems of N–Ti and N–Cu at incident energies between 10 and 1000 MeV.

4. Double *K*-shell ionization

As is described in the Sec. 1, the intensity ratio of hypersatellite and satellite K_α x-rays $I = \Sigma X(K^2L^n)/\Sigma X(KL^n)$ were previously obtained at RIKEN by Awaya et al. [13] for Ti targets and the projectiles of He, C, N, and O ions at 4.7–7.7 MeV/u. The ratio have been further obtained for 26 MeV/u N-ion impact on Ti, Fe, Ni, and Cu targets, and 92 MeV/u Ar-ion impact on Ti, Cr, Fe, Ni, and Cu targets.

Among the previously obtained data, the results of C- and N-ion bombardments are included in the following discussions. The hypersatellite x rays from the target were scarcely observed in the present work when the incident energy of ions was lower than 2.4 MeV/u.

4.1. Experimental results

The experimental *I* values including the previous data are plotted against $E/\lambda u_K$ in Fig. 7, where *E* is the total incident energy of projectiles, λ is the projectile mass in unit of electron mass and u_K is the binding energy of a target *K* electron. The parameter $E/\lambda u_K$ is roughly equal to $(v_i/v_K)^2$ where v_K is the orbital velocity of the target *K* electron. The values of *I* for C ions and for Ar ions are scaled by Z_1^2 to the N-ion projectile with the same velocities, that is, the data is multiplied by $(7^2/6^2)$ and $(7^2/18^2)$, respectively. According to Eq. (6), the scaling factor of $u_K(Z_2)/u_K(\mathrm{Ti})$ was multiplied by the values of V, Cr, Fe, Ni, and Cu targets. The experimental

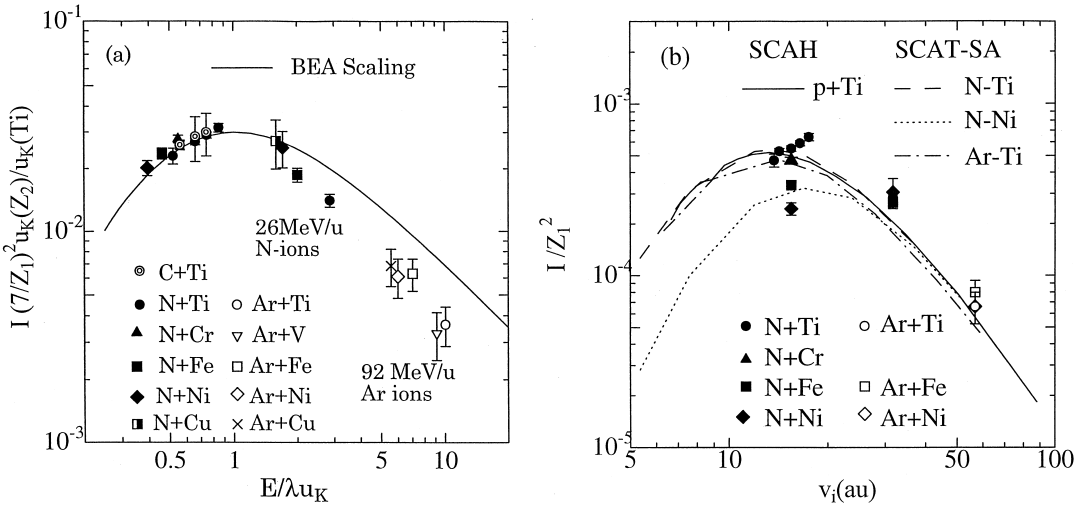

Fig. 7. (a) The intensity ratio between hypersatellites and satellites, I, normalized to N–Ti system and scaled by $Z_1^2 u_K(Z_2)$ as a function of $E/\lambda u_K$. The solid curve is K ionization cross section from BEA scaling normalized to the experimental data at $E/\lambda u_K = 1$. (b) The intensity ratio I divided by the projectile charge squared (Z_1^2) as a function of v_i. The curves show the results of SCA calculations by Hansteen et al. [29] (SCAH) and Trautmann and Rösel [30] (SCAT-SA).

data are obtained directly from the yields of both hypersatellite and satellite x rays and are not corrected for the fluorescence yields of each K^2L^n x rays and KL^n x rays. Numerical values of I are shown in Table 2.

The uncertainty comes mainly from the statistics and the estimation of the background caused by the Compton scattering of γ rays which were induced by the nuclear reactions and incident to the PSPC directly. Errors of I range from 20% to 30% for the cases of 6 and 6.75 MeV/u C ion on Ti, 26 MeV/u N ion on Ni and Cu, and 92 MeV/u Ar on all the targets. In other cases, it ranges from 3% to 10%.

As is seen in Fig. 7, all the experimental data shows a systematic dependence on the incident energy when we adopted the BEA scaling of the Z_1, Z_2, and E.

4.2. Fluorescence yield and intensity distributions

The fluorescence yield for initial states with double K and n L vacancies, $\omega_{2K,nL}$ and that with single K and n L vacancies, $\omega_{K,nl}$ were calculated for Ar ions by Zou et al. [34]. The values of $\omega_{2K,nL}$ is larger than $\omega_{K,nL}$ by 5.5%, 5.0%, 5.2%, and 5.8% for the n (in $2p$ state) = 0, 1, 2, 3 and no $2s$ vacancies, respectively. Though the target elements are a little heavier than Ar, we assumed that the relation between the $\omega_{2K,nL}$ and $\omega_{K,nL}$ is similar to the present target elements. In the present measurements as well as previous ones, strong lines among the K^2L^n and KL^n ones are those with $n = 0$, 1, and 2. As the difference between the calculated value of $\omega_{2K,nL}$ and that of $\omega_{K,nL}$ is almost constant and is within the experimental error in the present measurements, we assume that $\omega_{2K,nL} \simeq \omega_{K,nL}$ for the same value of n.

Olsen and Moore [8] observed that the structure of hypersatellite K_α and satellite K_α x rays is similar to each other, that is, the value of P_L for hypersatellite lines and that for satellite lines is almost same. This is the same in our case, as is seen in Fig. 1(a) and (b), as well as the previous data [12].

Since the intensity of the hypersatellite x rays is lower than 4% of that of satellite x rays, the contribution of single K vacancy from the de-excitation of double K vacancies can be neglected when we consider the error of the measurements.

4.3. Comparison of experimental results with calculations

According to the discussions in the previous subsection, we can consider that $\Sigma X(K^2L^n)/\Sigma X(KL^n)$ is roughly equal to $\sigma(K^2)/\sigma(K)$, where $\sigma(K^2)$ is the double K ionization and $\sigma(K)$ the single K ionization cross section. When the ionization probability is assumed to be constant, that is, it takes an average value of K-ionization probability, then the curve of $\sigma(K^2)/\sigma(K)$ shows similar dependence on $E/\lambda u_K$. The ionization cross section from BEA, which is normalized to the experimental data, is shown by the solid line in Fig. 7 for comparison. The experimental values decrease more rapidly in the range of $E/\lambda u_K > 1$ than the BEA curve, but it roughly follows the experimental data. The similar tendency was obtained by Fujimoto et al. [9] for He ions on a Be target, where the yield of hypersatellite x rays decreases more strongly compared to that of satellite ones in the region of $E/\lambda u_K > 1$.

We made calculations of $\sigma(K^2)/\sigma(K)$ based on SCAH and SCAT-SA. The single K-ionization probability, $2P_K(b)$, is calculated as a function of the impact parameter b, where the factor of 2 is from the number of K electrons. The SCAH calculation is for a proton projectile on Ti, whereas the SCAT-SA calculations were performed for N^{7+} + Ti, N^{7+} + Ni, and Ar^{18+} + Ti collision systems. The ionization process is assumed to be independent between the two K electrons; thus, the ratio $\sigma(K^2)/\sigma(K)$ is expressed as

$$\frac{\sigma(K^2)}{\sigma(K)} = \int_0^\infty 2\pi P_K(b)^2 b db \Big/ \int_0^\infty 2\pi 2P_K(b) b db \tag{10}$$

where a contribution of $P_K(b)^2$ is neglected in the denominator. In the SCAT calculations, the effective charge of the target was assumed to be $Z_2 - 0.3$.

The results are compared with experimental results in Fig. 7(b) as functions of the collision velocity. The results of SCAH are plotted directly whereas those from the results of experiment and SCAT-SA calculations are divided by Z_1^2. The SCAT-SA calculations of $\sigma(K^2)/\sigma(K)$ for N–Ti and Ar–Ti collisions give nearly the same results as the SCAH calculation when they are scaled by $1/Z_1^2$. However, it should be noted that the SCAT-SA calculation for Ar–Ti yields unphysical results of $P_K(b) > 1$ at small b and low v_i.

The experiments at 6 MeV/u ($v_i = 15.5$) for N projectile on different targets reveal that the ratios for the heavier targets are lower than the lighter ones. This tendency is qualitatively reproduced by the SCAT-SA calculation which yields lower $\sigma(K^2)/\sigma(K)$ for the heavier target at $v_i < 28$. These collision velocities are lower than the K-electron velocity. However the calculations cannot reproduce the energy dependence of the experimental results for N–Ti at $13.7 < v_i < 17.5$.

On the other hand, at higher velocities, all the (normalized) theoretical ratios converge to a common curve independent of the target and the projectile. This is in good agreement with the experimental results for N ions at 26 MeV/u and Ar ions at 92 MeV/u where values of I/Z_1^2 are almost independent of the target.

5. Conclusions

We have presented experimental results of target L-shell ionization probability P_L at small impact parameter by ions of $2 \le Z_1 \le 18$ and $4.8 \le v_i \le 56.8$, obtained from intensity distributions of KL^n x rays.

The general behavior of the L-ionization probability P_L agree the BEA scaling with the GVG universal function, for different projectile-target combinations and a wide range of the scaled collision velocity between $2 < V < 9.5$. It means that the inner-shell ionization is explained by a two-body collision between an incident ion acting as a point charge and an independent target electron, when the collision velocity is larger than the orbital velocity of the ionized electron. It also means that the relation Eq. (4) holds for wide range of v_i and collision systems with a cutoff radius almost independent of v_i.

The agreement between the experiments and the GVG curve becomes worse at lower velocities $V < 2$, where the binding and coulomb deflection effects are expected to influence the ionization process.

The experimental P_L value for a Ti target agrees with the L-ionization probability calculated by SCA at small impact parameters for projectiles with $2 \leq Z_1 \leq 18$ when the collision velocity is higher than v_L. At lower velocities, the experimental results are much smaller than the SCA calculation with separated-atom target wave function, and they are well reproduced when a united-atom target wave function is used in the same calculation.

The both first-order theories, SCA and BEA are found to reproduce the overall behavior of the L-ionization probabilities for the collision systems investigated here when the collision velocity is higher than the orbital velocity of the target L electrons, although the absolute values of the experimental probabilities deviate from the predictions by about 20% for most cases.

The intensity ratio between hypersatellite and satellite K_α X-rays from the target, $I = \Sigma X(K^2L^n)/\Sigma X(KL^n)$ is obtained for C, N, and Ar projectiles at $13.7 \leq v_i$. This ratio is deemed to be nearly equal to the ratio of the double to the single K ionization cross section, $\Sigma X(K^2L^n)/\Sigma X(KL^n) \simeq \sigma(K^2)/\sigma(K)$. The experimental results plotted as a function of $E/\lambda u_K$ are compared with the K-shell ionization cross section from BEA, and cross-section ratios from SCA (SCAH, SCAT-SA, and SCAT-UA). All the calculations roughly fit to the experimental data, showing a maximum at collision velocity v_i close to the target K-electron velocity. It supports the description that the double K ionizations are independent ionizations of K electrons. Especially, at very high velocities ($v_i \gg v_K$), the ratio normalized by Z_1^2 becomes almost independent of both the target and the projectile which is in good agreement with the experimental data.

Acknowledgements

Thanks are due to Dr. T. Mizogawa, Dr. A. Hitachi, and Dr. B. Sulik for their help in the experiments and to Ms. M. Nishida for processing the data. The authors are obliged to Professor D. Trautmann for the use of his SCA codes.

References

[1] P. Richard, I.L. Morgan, T. Furuta, D. Burch, Phys. Rev. Lett. 23 (1969) 1009.
[2] A.R. Knudson, D.J. Nagel, P.G. Burkhalter, K.L. Dunning, Phys. Rev. Lett. 26 (1971) 1149.
[3] D. Burch, P. Richard, R.L. Blake, Phys. Rev. Lett. 26 (1971) 1355.
[4] R.L. Kauffman, J.H. McGuire, P. Richard, C.F. Moore, Phys. Rev. A 8 (1973) 1233.
[5] P. Richard, R.L. Kauffman, J.H. McGuire, C.F. Moore, D.K. Olsen, Phys. Rev. A 8 (1973) 1369.
[6] C. Schmiedekamp, B.L. Doyle, T.J. Gray, R.K. Gardner, K.A. Jamison, P. Richard, Phys. Rev. A 18 (1978) 1892.
[7] T. Tonuma, Y. Awaya, T. Kambara, H. Kumagai, I. Kohno, S. Özkök, Phys. Rev. A 20 (1979) 989.
[8] D.K. Olsen, C.F. Moore, Phys. Rev. Lett. 33 (1974) 194.
[9] F. Fujimoto, K. Kawatsura, K. Ozawa, M. Terasawa, Phys. Lett. 57A (1976) 263.
[10] K. Kawatsura, K. Ozawa, F. Fujimoto, M. Terasawa, Phys. Lett. 64A (1977) 282.
[11] Y. Awaya, Electronic and Atomic Collisions, Proceedings of ICPEAC XI, N. Oda, T. Takayanagi (Eds.), North-Holland, Amsterdam, 1979, p. 325.
[12] Y. Awaya, M. Akiba, T. Katou, H. Kumagai, Y. Tendow, K. Izumo, T. Takahashi, A. Hashizume, M. Okano, T. Hamada, Phys. Lett. 61A (1977) 111.
[13] Y. Awaya, T. Katou, H. Kumagai, T. Tonuma, Y. Tendow, K. Izumo, A. Hashizume, T. Takahashi, T. Hamada, Phys. Lett. 75A (1980) 478.
[14] Y. Awaya, Y. Kanai, T. Kambara, T. Mizogawa, A. Hitachi, B. Sulik, Spectroscopy and Collisions of Few Electron Ions, Proceedings of the Study Conference SCOFEI '88, M. Ivascu, V. Florescu, V. Zoran (Eds.), World Scientific, Singapore, 1989, p. 462.
[15] A. Hitachi, H. Kumagai, Y. Awaya, Nucl. Instrum. Methods 195 (1982) 631.
[16] F.P. Larkins, J. Phys. B: Atom. Molec. Phys. 4 (1971) L29.
[17] J.H. Scofield, Phys. Rev. A 9 (1974) 1041.
[18] M.H. Chen, B. Crasemann, H. Mark, At. Data Nucl. Data Tables 34 (1979) 13.
[19] C.P. Bhalla, Phys. Rev. A 8 (1973) 2877.
[20] M. Gryziński, Phys. Rev. 138 (1965) A305.
[21] M. Gryziński, Phys. Rev. 138 (1965) A322.
[22] M. Gryziński, Phys. Rev. 138 (1965) A336.
[23] J.H. McGuire, P. Richard, Phys. Rev. A 8 (1973) 1374.
[24] L. Vriens, Proc. Phys. Soc. 90 (1967) 935.
[25] G. Basbas, W. Brandt, R. Laubert, Phys. Rev. A 7 (1973) 983.
[26] W. Brandt, G. Lapicki, Phys. Rev. A 20 (1979) 465.
[27] J.A. Doggett, L. Spencer, Phys. Rev. 103 (1956) 1597.
[28] J.M. Hansteen, High-Energy Ion-Atom Collisions, Proceedings of the 3rd Workshop on High-Energy Ion-Atom Collisions, D. Berényi, G. Hock (Eds.). Springer-Verlag, Berlin, 1988, p. 39.

[29] J.M. Hansteen, O.M. Johnsen, L. Kocbach, At. Data Nucl. Data Tables 15 (1975) 305.
[30] D. Trautmann, F. Rösel, Nucl. Instrum. Methods 169 (1980) 259.
[31] P. Rymuza, Th. Stöhlker, C.L. Cocke, H. Geissel, C. Kozhuharov, P.H. Mokler, R. Moshammer, F. Nickel, C. Scheidenberger, Z. Stachura, J. Ullrich, A. Warczak, J. Phys. B: At. Mol. Opt. Phys. 26 (1993) L169.
[32] R. Schuch, Y. Awaya, T. Kambara, T. Mizogawa, Y. Kanai, H. Shibata, K. Shima, Z. Phys. D: At. Mol. Clusters 4 (1987) 339.
[33] T. Kambara, T. Mizogawa, Y. Awaya, Y. Kanai, R. Schuch, K. Shima, D. Trautmann, J. Phys. Soc. Jpn. 58 (1989) 3929.
[34] Y. Zou, Y. Awaya, C.P. Bhalla, T. Kambara, Y. Kanai, M. Oura, Y. Nakai, K. Ando, A. Hitachi, S. Kravis, Phys. Rev. A 51 (1995) 3790.